This is a repository copy of *Referenced compressed sensing for accurate and fast spatio-temporal signal reconstruction*.

White Rose Research Online URL for this paper:
http://eprints.whiterose.ac.uk/149000/

Version: Published Version

eprints@whiterose.ac.uk
https://eprints.whiterose.ac.uk/

Referenced compressed sensing for accurate and fast spatio-temporal signal reconstruction

Wattanit Hotrakool
Charith Abhayaratne

Referenced compressed sensing for accurate and fast spatio-temporal signal reconstruction

Wattanit Hotrakool and Charith Abhayaratne*
The University of Sheffield, Department of Electronic and Electrical Engineering, Sheffield, United Kingdom

Abstract. We address two challenges of applying compressed sensing in a practical application, namely, its poor reconstruction quality and its high computational complexity. Since most signals are not fully sparse in practice, the reconstructed signals from conventional reconstruction methods often suffer from reconstruction artifacts due to the distortion of small coefficients. To improve the reconstruction quality, we introduce referenced compressed sensing (RefCS), a reconstruction method that exploits the spatial and/or temporal redundancy between a pair of signals. We show that using a correlated reference—an arbitrary signal close to the compressed signal—there exists the bound of reconstruction error that depends on the distance between the reference and the signal. By exploiting the correlated reference, RefCS can improve the reconstruction quality by up to 90% in terms of peak signal-to-noise ratio. Moreover, it is possible to reduce the computational complexity of the proposed RefCS using the least squares method. The least squares reconstruction results can be obtained with quality comparable to that of iterative algorithms by employing the correlated reference. Using the least squares method improves the reconstruction time by a factor in the range of 9 to 5.4×10^4 according to our experiments. © *2019 SPIE and IS&T* [DOI: 10.1117/1.JEI.28.4.043010]

Keywords: compressed sensing; sparse reconstruction; correlated reference; the least squares.

Paper 190050 received Jan. 28, 2019; accepted for publication Jun. 19, 2019; published online Jul. 12, 2019.

1 Introduction

Compressed sensing (CS) is a signal acquisition paradigm that allows acquisition of full-length signals from under-sampled measurements. Since it was introduced by Candès et al.[1] and Donoho,[2] compressed sensing has become of interest in many fields of research. The main promise of compressed sensing is the ability to perform sub-Nyquist sampling by exploiting the sparsity of compressible signals. In compressed sensing, the essential information to reconstruct a sparse signal is contained in a small set of significant elements, whereas the other elements are zero or have very small magnitudes. The aim of compressed sensing is to acquire these significant elements directly using a fewer number of measurements than those stated by the Shannon/Nyquist theorem.[3]

Compressed sensing consists of two major operations: the sensing operation $\mathfrak{S}$ and the reconstruction operation $\mathfrak{R}$. Let $\mathbf{u} \in \mathbb{R}^n$ be an n-dimensional nonsparse signal that can be represented as an n-dimensional sparse signal, $\mathbf{x} \in \mathbb{R}^n$, via $\mathbf{x} = \Psi\mathbf{u}$ transformation using a sparse dictionary Ψ. The sensing operation $\mathfrak{S}(\mathbf{x})$ acquires the compressive measurements $\mathbf{y} \in \mathbb{R}^m$, where $m \ll n$, as follows:

$$\mathbf{y} = \Phi\mathbf{x}, \tag{1}$$

where $\Phi \in \mathbb{R}^{m \times n}$ is the incoherent under-sampling matrix. Generally, $\mathfrak{S}(\mathbf{x})$ is a linear equation. The incoherence of Φ to the signal $\mathbf{x}$—more specifically the incoherence between Φ and Ψ—is guaranteed by many properties including the null space property[4] and the restricted isometry property,[5,6] to name a few. As shown by Kim and Shevlyakov,[7] random sampling matrices are largely incoherent to every dictionary

Ψ, thus the random matrices are a widely used sampling operator.

The counterpart of the sensing operation is the reconstruction operation $\mathfrak{R}(\mathbf{y})$. The reconstruction operation recovers a full-length signal $\hat{\mathbf{x}} \in \mathbb{R}^n$ from the measurements $\mathbf{y}$. Because Eq. (1) is under-determined, the reconstruction cannot be done linearly. Instead, the reconstruction operation is an optimization problem aims to minimize a specific objective function. Conventionally, the CS reconstruction is done by minimizing the l_1-norm objective function, i.e.,

$$\min_{\hat{\mathbf{x}}} \|\hat{\mathbf{x}}\|_1 \quad \text{subject to } \Phi\hat{\mathbf{x}} = \mathbf{y}. \tag{2}$$

This reconstruction method is commonly known as the l_1-norm minimization (l_1-min for short). It is shown by Donoho[2] that when the sparsity of a signal is promoted by minimizing the l_1-norm objective function, the reconstructed signal can be obtained accurately with high probability. Finally, the original signal is reconstructed using the inverse transformation $\hat{\mathbf{u}} = \Psi^{-1}\hat{\mathbf{x}}$.

Conventionally, compressed sensing reconstructs a full-length signal from highly under-sampled measurements by solving the l_1-norm minimization problem. However, this has a couple of limitations. First, the l_1-norm minimization problem has to be solved using iterative optimization algorithms, which have high computational complexity. This complexity makes the time required for full-length signal reconstruction is too large to be desirable in most practical applications. The problem worsens with the increase of the signal length, preventing compressed sensing to be applicable to most data-intensive, next-generation content. Second, the reconstructed signal $\hat{\mathbf{x}}$ obtained by minimizing the signal sparsity using the l_1-norm minimization tends to lose small

*Address all correspondence to Charith Abhayaratne, E-mail: c.abhayaratne@sheffield.ac.uk
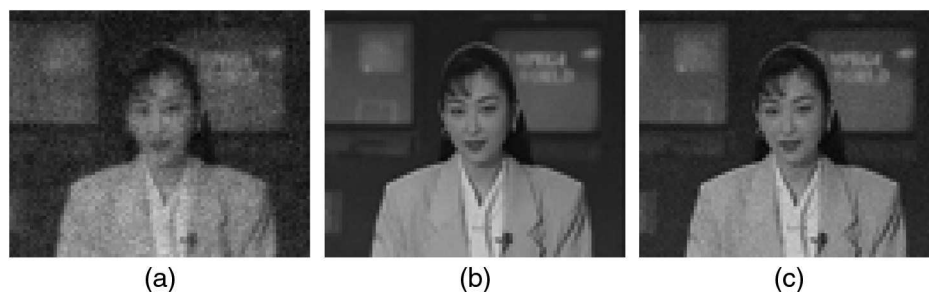
Fig. 1 Illustration of improvements due to the proposed methods RefCS and RefCS/LS: (a) l_1-min, (b) RefCS, and (c) RefCSLS.

magnitude components in the sparse signal representation domain **x**. As most of these smaller magnitude components are highly likely to be in high frequencies according to transform coefficients' characteristics, the final reconstructed signal **û** may be distorted with losing details, thus resulting in noise-like reconstruction artifacts in the reconstructed signal. Figure 1(a) shows such artifacts, which are clearly visible in a video sequence reconstructed using the l_1-norm minimization. This poses a challenge in many real-world applications, such as medical imaging, in which the high-frequency details are important and cannot be discarded.

This paper has two major contributions. The first contribution is the proposal of an approach for reconstruction in Sec. 3 in order to improve the CS reconstruction quality of the full-length signal by exploiting the redundancy between the signal **x** and a correlated reference **r**. Thus herein we call the proposed method referenced compressed sensing (RefCS). In this paper, we propose the theoretical foundations of RefCS and demonstrate it experimentally on how to exploit intersample redundancy for improving reconstruction quality. Let $\mathbf{x} \in \mathbb{R}^n$, be a sparse n-dimensional signal, which is acquired using compressive measurements $\mathbf{y} \in \mathbb{R}^m$, where $m \ll n$ and $\mathbf{y} = \Phi\mathbf{x}$, where $\Phi \in \mathbb{R}^{m \times n}$ is the incoherent under-sampling matrix. Suppose there is an *a priori* correlated reference signal **r** close to **x** in the sense that δ, the distance between **r** and **x**, i.e., $\delta = \|\mathbf{r} - \mathbf{x}\|_2$, is very small. RefCS proposes that the reconstructed signal **x̂** is the solution of

$$\min_{\hat{\mathbf{x}}} \|\hat{\mathbf{x}} - \mathbf{r}\|_1 \quad \text{subject to} \quad \Phi\hat{\mathbf{x}} = \mathbf{y} \tag{3}$$

and it obeys the constraint

$$\|\hat{\mathbf{x}} - \mathbf{x}\|_2 \leq 2\delta. \tag{4}$$

There is no other assumption about the relationship between **r** and **x** apart from the distance. Exploiting the redundancy between **r** and **x** leads to a much higher reconstruction quality [Fig. 1(b)]. Using the correlated reference **r**, the reconstructed data using the proposed RefCS are shown to have higher peak signal-to-noise ratio (PSNR) values than the those for the traditional l_1-norm minimization reconstruction. In this work, the performance of RefCS is demonstrated in three different applications: multiscale image reconstruction, video reconstruction, and functional magnetic resonance imaging (fMRI) data with PSNR improvements of 5.43%, 40%, and 90%, respectively, as shown in Sec. 5. For video reconstruction, unless motion compensated, it is usually difficult to find a highly correlated reference from

the previously decoded data. As shown in Sec. 5, the performance improvement for sequences with high-motion content is not as high as for those with less motion content.

The second contribution of this paper is a solution for the issue of high-reconstruction complexity of compressed sensing as presented in Sec. 4. We show that it is possible to reconstruct the full-length signal using the l_2-norm objective function with the least squares method by incorporating the correlated reference **r**. Provided Φ is a full rank matrix, the reconstructed signal **x̂** can be obtained as

$$\hat{\mathbf{x}} = \mathbf{r} + \Phi^{\mathrm{T}}(\Phi\Phi^{\mathrm{T}})^{-1}(\mathbf{y} - \Phi\mathbf{r}). \tag{5}$$

Thus hereinafter, we call the proposed solution in Sec. 4 referenced CS with the least squares (RefCSLS). The reconstructed data from RefCSLS approach have resulted in quality comparable to that of regular RefCS reconstruction that uses l_1-norm [Fig. 1(c)], but with low computational times. As shown in Sec. 5, it yields PSNR improvements of 5.83% in multiscale image reconstruction, 18% in video reconstruction, and 89% in fMRI data with great reductions of computational time compared to the iterative algorithms used in l_1-norm minimization.

The remainder of this paper is organized as follows: the related work is discussed in Sec. 2. The proposed RefCS is introduced in Sec. 3, followed by the low-complexity variant RefCSLS in Sec. 4. The experimental results, including all three example application scenarios, are presented in Sec. 5 followed by concluding remarks in Sec. 6.

2 Related Work

A priori side-information regarding the structure of signals has been explored within the CS sensing and reconstruction operations in the literature. The main motivation of CS reconstruction methods employing side-information is the fact that the characteristics and structure of a signal are shared between its neighbors. This observation can be seen clearly in applications, such as, in magnetic resonance imaging (MRI),[8,9] sensor network,[10] multiview imaging,[11] and surveillance camera,[12] etc. Since Miosso et al.[13] showed that the use of side information can reduce the number of measurements required, various side-information types have been studied and incorporated into the CS reconstruction operation.[14] Examples include sparsity patterns (including these variants: sparse support estimation,[15] model-based CS,[16] and Kalman-filtered CS[17]), upper and lower bounds,[18] and joint/group reconstruction.[11]

Video data contain a high level of temporal redundancy between frames that can be employed as side information.

The interframe redundancy is at the heart of video compression techniques. It is also exploited in distributed video coding (DVC) to achieve coding gains.[19–21] DVC views consecutive frames as a corrupted version of a key frame and uses the key frame as the base for reconstructing the corrupted frame. Previous works in the literature show improvements in distributed compressive video sensing (DCVS) over the traditional CS reconstruction.[22–24] There also presents the attempt to incorporate the intraframe redundancy (which is the spatial redundancy) into the reconstruction method.[25] The generalized version of DCVS leads to the development of a more dynamic approach to video sequence reconstruction, known as temporal compressed sensing (TCS).[26–29] TCS reconstructs a signal by maximizing the sparsity as well as exploiting the redundancy between two consecutive reconstructed frames in a spatio-temporal signal. In other words, TCS solves the following problem:

$$\min_{\hat{\mathbf{x}}}(\|\hat{\mathbf{x}}_t\|_1 + \|\Psi^{-1}\hat{\mathbf{x}}_t - \Psi^{-1}\hat{\mathbf{x}}_{t-1}\|_1) \quad \text{subject to } \Phi\hat{\mathbf{x}}_t = \mathbf{y}, \quad (6)$$

corresponding to the two consecutive frames $\mathbf{u}_t$ and $\mathbf{u}_{t-1}$, where $\mathbf{x}_t = \Psi\mathbf{u}_t$ and $\mathbf{x}_{t-1} = \Psi\mathbf{u}_{t-1}$, respectively. Unlike DCVS, TCS does not restrict the use of a key frame as a base for reconstruction. Instead, the most recent reconstructed frame is used directly as a base for the next frame.

The concept of reconstruction based on redundancy is applicable not only to video sequence reconstruction[30] but also to many similar applications, such as block-based image processing[31] and phase-based remote sensing.[32] These involve measurements of a large signal as a collection of several smaller subsignals, i.e., each individual block in the image processing, each frame in the video reconstruction, and each phase-component in remote sensing. These smaller subsignals have a high degree of redundancy and are highly correlated to each other, which is exploited in the reconstruction or processing stage.

In all above work, interpixel redundancy has been exploited by considering special application scenarios to improve the quality of the reconstructed data. In the proposed RefCS, a generalized and application-independent approach to exploit interpixel redundancy by means of a correlated reference is formulated. The early findings of our work were reported in two conference publications.[33,34] In this work, we propose the mathematical formulation of RefCS and its extension into the least square reconstruction (RefCSLS), analyze the effect of the correlated reference and sampling rate on reconstruction errors, and experimentally evaluate the proposed method considering three example application scenarios: image, video, and fMRI data reconstruction. More detailed analysis, experimental evaluation, and other applications of our work can be found in the PhD thesis of the first author.[35]

3 Referenced Compressed Sensing

3.1 Proposed Reconstruction Operation

A large signal, such as, an image or a video sequence can be viewed as a collection C consisting of several smaller subsignals. Concretely, a subsignal $\mathbf{x}_t \in \mathbb{R}^n$, $t = 1, 2, \ldots, k$ is a member of the collection $C_{\mathbf{x}}$, where n is the length of each signal $\mathbf{x}_t$ and k is the total number of $\mathbf{x}_t$ in $C_{\mathbf{x}}$. In RefCS, the correlated reference $\mathbf{r}$ is not required to be from the same collection as $\mathbf{x}$, i.e., the condition $\mathbf{r} \in C_{\mathbf{x}}$ is not required. In RefCS, a correlated reference $\mathbf{r}$ is an arbitrary signal close to $\mathbf{x}$, as defined in Definition 3.1.

Definition 3.1. For any signal $\mathbf{x} \in \mathbb{R}^n$, a correlated reference $\mathbf{r}$ of $\mathbf{x}$ is a signal such that $\mathbf{r} \in \mathbb{R}^n$ and

$$\|\mathbf{r} - \mathbf{x}\|_2 \leq \epsilon, \quad (7)$$

for a small $0 < \epsilon \ll \|\mathbf{x}\|_2$.

The reference distance $\delta = \|\mathbf{r} - \mathbf{x}\|_2$ has a very important role in RefCS. Though the correlated reference $\mathbf{r}$ is arbitrary, it is possible to find an orthogonal projection of $\mathbf{r}$ on the feasible set $\hat{\mathbf{X}}_{\Phi,\mathbf{y}}$ given by the constraints of Eq. (1).

Proposition 1. Given a sensing matrix $\Phi \in \mathbb{R}^{m \times n}$, a compressive measurement $\mathbf{y} \in \mathbb{R}^m$, $\mathbf{y} = \Phi\mathbf{x}$, and a correlated reference $\mathbf{r} \in \mathbb{R}^n$, an orthogonal projection $\hat{\mathbf{x}}_P$ from $\mathbf{r}$ onto the feasible subspace $\hat{\mathbf{X}}_{\Phi,\mathbf{y}} = \{\hat{\mathbf{x}}|\mathbf{y} = F\mathbf{x}\}$ satisfies

$$\sup_{\hat{\mathbf{x}}_P}\|\hat{\mathbf{x}}_P - \mathbf{x}\|_2 \leq \delta. \quad (8)$$

Proof. Consider the case of $\mathbf{x} \in \mathbb{R}^2$ in Fig. 2. Let a reference $\mathbf{r}$ be a member of a set of references R, such that $R = \{\mathbf{r} : \|\mathbf{r} - \mathbf{x}\|_2 \leq \delta\}$. Also, define an orthogonal projection $\hat{\mathbf{x}}_P$, which is the projection of the reference $\mathbf{r} \in R$ onto the feasible subspace $\hat{\mathbf{X}}_{\Phi,\mathbf{y}}$. ☐

Let $L = \|\hat{\mathbf{x}}_P - \mathbf{r}\|_2$ be the length of the projection. One finds that

$$L \leq \delta \sin \theta, \quad (9)$$

where θ is the angle between $\mathbf{r} - \mathbf{x}$ and $\mathbf{x}_P - \mathbf{x}$. Because of the relationship

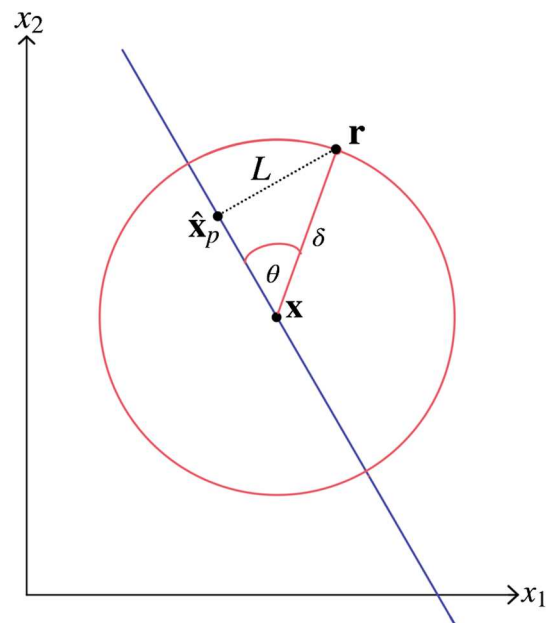$$\|\hat{\mathbf{x}}_P - \mathbf{x}\|_2^2 = \delta^2 - L^2, \quad (10)$$

Fig. 2 Geometric example of Proposition 1, where $\mathbf{x} \in \mathbb{R}^n$.

we can see that $\|\hat{\mathbf{x}}_P - \mathbf{x}\|_2$ is maximized when $L = 0$, i.e., $\theta = 0$. This implies that, for any $\mathbf{r} \in R$,

$$\sup_{\hat{\mathbf{x}}_P} \|\hat{\mathbf{x}}_P - \mathbf{x}\|_2 \leq \delta. \qquad (11)$$

In the proposed RefCS, instead of using the orthogonal projection as in Proposition 1, the solution $\hat{\mathbf{x}}_1$ can be obtained using the l_1-norm minimization. In this case, the sparsity of $\hat{\mathbf{x}}_1$ is promoted.

Proposition 2 Given a sensing matrix $\Phi \in \mathbb{R}^{m \times n}$, a compressive measurements $\mathbf{y} \in \mathbb{R}^m$, $\mathbf{y} = \Phi\mathbf{x}$, and a correlated reference $\mathbf{r} \in \mathbb{R}^n$, a least l_1-norm reconstruction $\hat{\mathbf{x}}_1$, which is the solution of

$$\min_{\hat{\mathbf{x}}} \|\hat{\mathbf{x}} - \mathbf{r}\|_1 \quad \text{subject to } \Phi\hat{\mathbf{x}} = \mathbf{y}, \qquad (12)$$

satisfies

$$\|\hat{\mathbf{x}}_1 - \mathbf{x}\|_2 \leq 2\delta. \qquad (13)$$

Proof. Consider the case of $\mathbf{x} \in \mathbb{R}^2$ in Fig. 3. Let a reference $\mathbf{r}$ be a member of a set of references R such that, $R = \{\mathbf{r} | \|\mathbf{r} - \mathbf{x}\|_2 \leq \delta\}$. The least l_1-norm solution $\hat{\mathbf{x}}_1$ is a point on the feasible subspace $\hat{\mathbf{X}}_{\Phi,\mathbf{y}} = \{\hat{\mathbf{x}} | \mathbf{y} = F\mathbf{x}\}$, such that, the norm $\|\hat{\mathbf{x}}_1 - \mathbf{r}\|$ is minimized. Define the angle between the vectors $\hat{\mathbf{x}}_1 - \mathbf{r}$ and $\hat{\mathbf{x}}_P - \mathbf{r}$ as ρ. Both $\hat{\mathbf{x}}_1$ and $\hat{\mathbf{x}}_P$ are on the feasible subspace $\hat{\mathbf{X}}_{\Phi,\mathbf{y}}$, because $\hat{\mathbf{x}}_P$ is an orthogonal projection, it is clear that

$$\|\hat{\mathbf{x}}_P - \mathbf{r}\|_2 \leq \|\hat{\mathbf{x}}_1 - \mathbf{r}\|_2. \qquad (14)$$

From Fig. 3, it can be seen that

$$\|\hat{\mathbf{x}}_1 - \hat{\mathbf{x}}_P\| = \|\hat{\mathbf{x}}_P - \mathbf{r}\|_2 \tan \rho. \qquad (15)$$
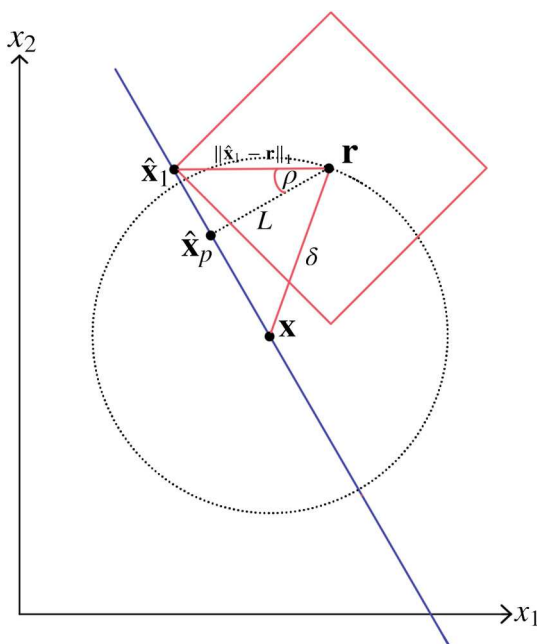
Fig. 3 Geometric example of Proposition 2, where $\mathbf{x} \in \mathbb{R}^n$.

From Proposition 1, we know that $\|\hat{\mathbf{x}}_P - \mathbf{r}\|_2 \leq \delta$. Also from Fig. 3, it can be seen that $\rho \leq \frac{\pi}{4}$ for $\hat{\mathbf{x}}_1$ to be the smallest l_1-norm solution, thus

$$\|\hat{\mathbf{x}}_1 - \hat{\mathbf{x}}_P\|_2 \leq \delta. \qquad (16)$$

This implies that

$$\sup_{\hat{\mathbf{x}}_1} \|\hat{\mathbf{x}}_1 - \mathbf{x}\|_2 = \|\hat{\mathbf{x}}_1 - \hat{\mathbf{x}}_P\|_2 + \|\hat{\mathbf{x}}_P - \mathbf{r}\|_2, \qquad (17)$$

$$= 2\delta. \qquad (18)$$

Both Proposition 1 and Proposition 2 show that the error of RefCS depends on the distance δ between the reference $\mathbf{r}$ and the signal $\mathbf{x}$.

3.2 Relationship Between Correlated Reference, Sampling Rate, and Reconstruction Error

As shown in Proposition 2, the performance of RefCS is governed by the reference distance $\delta = \|\mathbf{r} - \mathbf{x}\|_2$ between the correlated reference $\mathbf{r}$ and the signal $\mathbf{x}$. The goal is to minimize the reconstruction error $E(\hat{\mathbf{x}}, \mathbf{x}) = \|\hat{\mathbf{x}} - \mathbf{x}\|_2$.

First, let us consider the relationship between the distance δ and $E(\hat{\mathbf{x}}, \mathbf{x})$. To study this relationship, the Monte Carlo method is employed to a pool of signal $P = \{\mathbf{x} : \mathbf{x} \in \mathbb{R}^{256}\}$ containing 1000 linearly independent random vectors. Each vector $\mathbf{x}_i \in P$ has the number of nonzero elements fixed to 50, each element has the value between 0 and 255.

A set of 50 randomly chosen vectors $P_I \subset P$ is used as input signals. The sensing operation $\mathfrak{S}$ and reconstruction operation $\mathfrak{R}$, using RefCS, are applied to each signal $\mathbf{x} \in P_I$ repeatedly, each time using a different reference vector $\mathbf{r} \in P, \mathbf{r} \notin P_I$. Figure 4 shows the scatter plot of each reconstructed signal between δ against $E(\hat{\mathbf{x}}, \mathbf{x})$, along with their linear regression trend. Figure 4 clearly shows that the smaller reference distance δ indeed leads to the lower reconstruction error in general. Moreover, it can be seen that the reconstruction error is far lower than the limit imposed by Proposition 2. The reference distance δ in this experiment is unusually high compared to typical setting because vectors in each signal-reference pair $(\mathbf{x}, \mathbf{r})$ are independent of each
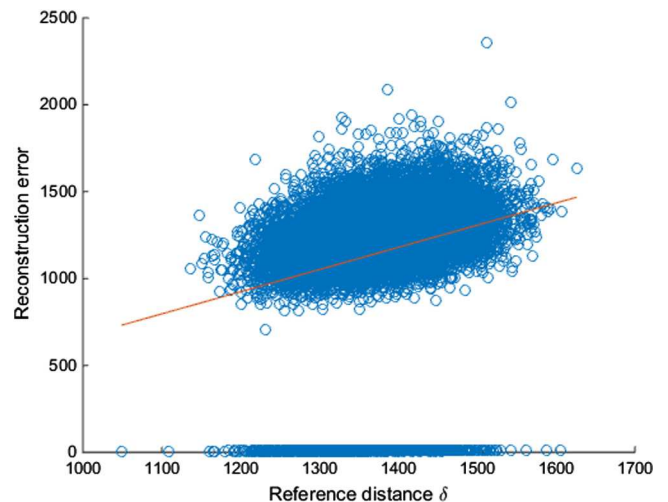
Fig. 4 Scatter plot showing the relationship between the reference distance δ and the reconstruction error $E(\hat{\mathbf{x}}, \mathbf{x})$ of RefCS.

other and share no redundancy. This is intentional in order to study the case where the reference is completely arbitrary. This scenario is of course not optimal, but, despite this extremity, the relationship between the reference distance and the reconstruction error is clear.

The next step is to study the relationship of the sampling rate s to the reconstruction error $E(\hat{\mathbf{x}}, \mathbf{x})$, given the references with fixed distance. Again, Monte Carlo method is employed onto the same pool of random vectors P. This time, the sensing operation $\mathfrak{S}$ and the reconstruction operation $\mathfrak{R}$ are applied to each vector $\mathbf{x} \in P$ repeatedly, each time using a different sampling rate s, where $10\% \leq s \leq 90\%$. The reference $\mathbf{r}$ is created by adding random noise to $\mathbf{x}$. Specifically, for each $\mathbf{x}$, we create a reference signal

$$\mathbf{r} = \mathbf{x} + k\mathbf{n}, \tag{19}$$

where $\mathbf{n}$ is a uniform white noise such that,

$$\|\mathbf{r} - \mathbf{x}\|_2 = k\|\mathbf{x}\|_2. \tag{20}$$

In this experiment, three values of k are chosen to create references at three distances: $\delta_L = 0.25\|\mathbf{x}\|_2$, $\delta_M = 0.5\|\mathbf{x}\|_2$, and $\delta_H = 0.75\|\mathbf{x}\|_2$.

Figure 5 shows the average plot between the sampling rate s and the error $E(\hat{\mathbf{x}}, \mathbf{x})$. As one would expect, the error goes up as the sampling rate decreases. However, the error also reduces as the distance δ decreases. Given the same sampling rate, it is clear that the results obtained using the smaller δ have a much lower error. In addition, the difference between the reconstruction error of low- and high-sampling rate is narrower with the smaller δ. Let E_s denote the reconstruction error at the sampling rate s. As shown in Fig. 5, the error difference is E_{10}–escaped;$E_{90} = 880.18$ when using the references with δ_H. On the other hand, the error difference reduces to 175.58 when reconstructed using the references with δ_L. In order words, the effect of the sampling rate to the reconstruction error is smaller when the reference distance is small.

Figure 5 also shows lines indicating the value twice the reference distance, i.e., 2δ, showing the limit imposed by Proposition 2. It shows that the RefCS results strictly obey Proposition 2.
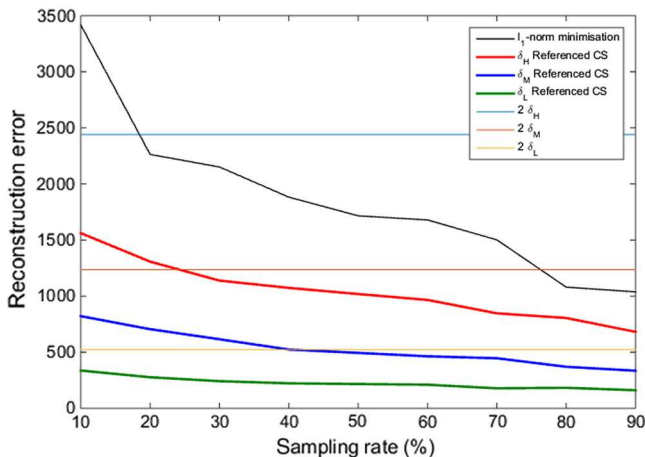
Fig. 5. Relationship between the sampling rate s, the reference distance δ, and the reconstruction error $E(\hat{\mathbf{x}}, \mathbf{x})$ of RefCS.

4 Reduction of Reconstruction Complexity: Referenced Compressed Sensing with the Least Squares

One of the major issues that prevents a practical deployment of compressed sensing is the high computational complexity of iterative reconstruction operation. High complexity makes the reconstruction of large data a time-consuming task. Here we propose a method that greatly reduces the complexity of CS reconstruction by relaxing the objective function of RefCS from l_1-norm to l_2-norm, thus allowing the reconstruction to be done using the least squares approximation.

This claim might come as a surprise as the l_2-norm objective is known to not promote the signal sparsity. However, one of the main promises of RefCS is the fact that it moves away from the notion of sparsity. Recall the same symbols from Sec. 3. As shown in Proposition 2, the reconstruction error $E(\hat{\mathbf{x}}, \mathbf{x})$ depends only on the distance $\delta = \|\mathbf{r} - \mathbf{x}\|_2$ between the reference $\mathbf{r}$ and the signal $\mathbf{x}$. This proposition is valid for any l_p-norm, $0 < p \leq \infty$. As the sparsity is no longer needed to be maximized, it is desirable to relax the optimization problem back to use the l_2-norm objective function to take advantage of its lower complexity.

Here we assert that the least squares method should perform reasonably well with the incorporation of the correlated reference since it is bounded by Proposition 2. As such, we propose to use the least squares method to solve for the solution of the relaxed RefCS, referred to as RefCS with the least squares (RefCSLS), following the Proposition 3.

Proposition 3. Given $\mathbf{r} \in \mathbb{R}^n$, a correlated reference of a signal $\mathbf{x} \in \mathbb{R}^n$, the reconstructed signal $\hat{\mathbf{x}} \in \mathbb{R}^n$ can be obtained from the compressive measurements $\mathbf{y} \in \mathbb{R}^m$, where $\mathbf{y} = \Phi\mathbf{x}$ and provided Φ is full rank matrix, as follows:

$$\hat{\mathbf{x}} = \mathbf{r} + \Phi^{\mathrm{T}}(\Phi\Phi^{\mathrm{T}})^{-1}(\mathbf{y} - \Phi\mathbf{r}) \tag{21}$$

Proof. Following Eq. (12), we define a RefCS l_2-norm minimization problem as

$$\min_{\mathbf{x}}\|\hat{\mathbf{x}} - \mathbf{r}\|_2 \quad \text{subject to } \Phi\hat{\mathbf{x}} = \mathbf{y}. \tag{22}$$

Define a Lagrangian function as

$$\mathcal{L}(\hat{\mathbf{x}}) = \|\hat{\mathbf{x}} - \mathbf{r}\|_2^2 + \lambda^{\mathrm{T}}(\Phi\hat{\mathbf{x}} - \mathbf{y}), \tag{23}$$

where λ is the Lagrange multipliers for the constraint set in a diagonal matrix in $\mathbb{R}^m$ and $^{\mathrm{T}}$ represents the transpose. Setting the derivative of $\mathcal{L}(\hat{\mathbf{x}})$ with respect to $\hat{\mathbf{x}}$ to zero:

$$\frac{\partial}{\partial\hat{\mathbf{x}}}\mathcal{L}(\hat{\mathbf{x}}) = 2\hat{\mathbf{x}} - 2\mathbf{r} + \lambda^{\mathrm{T}}\Phi = 0, \tag{24}$$

and considering the fact that $\Phi \in \mathbb{R}^{m \times n}$, we can rewrite Eq. (24) as

$$2\hat{\mathbf{x}} - 2\mathbf{r} + \Phi^{\mathrm{T}}\lambda = 0, \tag{25}$$

to obtain the condition

$$\hat{\mathbf{x}} = \mathbf{r} - \frac{1}{2}\Phi^{\mathrm{T}}\lambda. \tag{26}$$

To solve for the Lagrange multipliers λ, substitute Eq. (26) into $\mathbf{y} = \Phi\hat{\mathbf{x}}$ to obtain

$$\mathbf{y} = \Phi \mathbf{r} - \frac{1}{2} \Phi \Phi^T \lambda. \tag{27}$$

From Eq. (27), we get

$$\Phi \Phi^T \lambda = -2(\mathbf{y} - \Phi \mathbf{r}), \tag{28}$$

and, finally,

$$\lambda = -2(\Phi \Phi^T)^{-1}(\mathbf{y} - \Phi \mathbf{r}). \tag{29}$$

With the assumption of Φ as full rank, the matrix $\Phi \Phi^T$ is positive-definite and thus invertible. Substitute Eq. (29) back into Eq. (26) to obtain the expression in Eq. (21), i.e.,

$$\hat{\mathbf{x}} = \mathbf{r} + \Phi^T (\Phi \Phi^T)^{-1} (\mathbf{y} - \Phi \mathbf{r}). \tag{30}$$

□

Therefore, with the least square minimization approach, the reconstruction process reduces to the expression in Eq. (21). The experiments in terms of three case studies and

(a)   (b)   (c)   (d)   (e)

Fig. 6 Reconstructed images from 50% compressive measurements using (a) l_1-norm minimization, (b) RefCS using low-resolution (25%) references, (c) RefCS using low-resolution (6.25%) references, (d) RefCSLS using low-resolution (25%) references, and (e) RefCSLS using low-resolution (6.25%) references.

Table 1 Average PSNR in decibels of reconstructed multiscale images using the proposed reconstruction methods at the sampling rate of 10%, 30%, and 50%. The reference image R is at 25% and 6.25% of the original image.

Image	l_1-min			RefCS (large R)			RefCS (small R)			RefCSLS (large R)			RefCSLS (small R)		
	10%	30%	50%	10%	30%	50%	10%	30%	50%	10%	30%	50%	10%	30%	50%
Aerial	28.22	28.53	28.92	29.06	29.08	29.27	28.66	28.78	28.94	29.11	29.17	29.30	28.74	28.85	28.99
Baboon	29.73	29.89	30.22	30.56	30.71	31.01	29.79	30.00	30.54	30.71	30.83	30.98	29.84	30.08	30.45
Barbara	28.48	28.93	30.02	30.76	31.02	31.61	29.34	29.66	30.56	30.98	31.25	31.53	29.49	29.60	29.89
Boat	29.06	29.38	30.05	30.97	31.14	31.35	29.74	29.85	30.45	31.01	31.11	31.32	30.07	30.10	30.13
Cameraman	29.50	29.68	29.75	31.23	31.49	31.57	29.95	29.98	30.27	31.63	31.77	31.84	30.17	30.28	30.52
Gold hill	29.19	29.78	30.55	31.10	31.30	31.72	29.87	30.16	30.83	31.14	31.39	31.72	29.97	30.17	30.58
Peppers	28.00	28.61	29.30	30.57	30.68	31.23	29.07	29.48	29.93	30.86	30.89	31.40	29.26	29.37	29.69

discussion of the reconstruction quality and running times of RefCSLS method are presented in Sec. 5.

5 Experimental Results

In this section, three case studies where RefCS and RefCSLS can be employed are presented. They are multiresolution image reconstruction, video sequence reconstruction, and fMRI data reconstruction. Throughout these experiments, the infeasible-point subgradient algorithm,[36] which is one of the most efficient reconstruction methods available,[37] is used as the optimization algorithm for both the l_1-norm minimization and the regular RefCS.

5.1 Image Reconstruction

This section demonstrates the performance of the proposed RefCS and RefCSLS in a proof-of-concept scenario of multiscale image reconstruction. Let an image $\mathbf{I}$ consisting of n pixels be measured compressively using the sensing operation $\mathfrak{S}$. As discussed, the images reconstructed using l_1-norm minimization method have a significant amount of reconstruction artifacts, as shown in column (b) of Fig. 6.

In the image reconstruction scenario, the reference signal can come from a previously reconstructed neighboring group of pixels in a line considering line by line acquisition or from a previously acquired ultralow resolution version of the image. For this case study, the latter is considered for demonstrating the performance of proposed RefCS and RefCSLS. Suppose there is an ultralow resolution sensor that can capture a small reference image $\mathbf{R}$, where the size of $\mathbf{R}$ is much smaller than $\mathbf{I}$. Instead of measuring the entirety of m samples compressively as $\mathbf{y}$, the samples in this scenario contain two vectors: the reference image $\mathbf{R}$ and the random sample $\mathbf{y}$ (while keeping the total amount of samples at m). In this scenario, RefCS can employ the reference vector $\mathbf{r}$, where $\mathbf{r}$ is the sparse representation of the super-resolution version of $\mathbf{R}$, i.e., given that $\mathbf{x} = \Psi\mathbf{I}$,

$$\mathbf{y} = \Phi\Psi\mathbf{I}, \tag{31}$$

and the reference vector $\mathbf{r}$ is

$$\mathbf{r} = \Psi S(\mathbf{R}), \tag{32}$$

where $S(\mathbf{R})$ is the super-resolution operation. The reconstruction operation $\mathfrak{R}$ is employed to reconstruct the image $\hat{\mathbf{I}}$ by

$$\hat{\mathbf{x}} = \mathfrak{R}(\mathbf{y}, \mathbf{r}), \tag{33}$$

$$\hat{\mathbf{I}} = \Psi^{-1}\hat{\mathbf{x}}. \tag{34}$$

Figure 6 shows the reconstructed images using the RefCS and the RefCSLS using $\mathfrak{R}$. In columns of Figs. 6(b) and 6(d), the total samples $m = 0.5n$ consist of $0.25n$ from the low-resolution reference image $\mathbf{R}$ and $0.25n$ from the compressive measurements $\mathbf{y}$, where as in columns of Figs. 6(c) and 6(e), the samples $m = 0.5n$ consist of $0.0625n$ from the reference image $\mathbf{R}$ and $0.4375n$ from $\mathbf{y}$. It is clear in these examples that by employing the low-resolution reference, the reconstruction artifacts are reduced greatly. In this figure, the reconstructed images are far noisier compared to those in Fig. 6(b). However, Table 1 shows that both the reconstructed images in Figs. 6(b) and 6(c) have higher PSNR than the images obtained using the conventional l_1-norm minimization. When using a large reference image $\mathbf{R}$ ($0.25n$), the RefCS and RefCSLS results show the average improvement

Table 2 Average reconstruction time per image (s) of each reconstruction method.

Image	l_1-min	RefCS	RefCSLS
Aerial	11.63	11.58	1.22
Baboon	12.00	11.91	1.35
Barbara	11.88	11.83	1.23
Boat	11.69	11.79	1.24
Cameraman	11.92	12.24	1.26
Gold hill	12.13	11.99	1.27
Peppers	11.61	11.73	1.28

of 5.43% and 5.83%, respectively, compared to the l_1-norm minimization. When using a small **R** ($0.0625n$), the improvements are 1.71% and 1.76%, respectively. The reason that the RefCSLS results have better PSNR than the results of the regular RefCS, in this experiment, is because the lower reconstruction accuracy of RefCSLS—which results in blurring instead of the reconstruction artifacts—acts as a low-pass filter for the images that filter out the artifacts. While this outcome is not particularly desirable, Table 2 shows that RefCSLS, despite yielding the results comparable in reconstruction quality, is faster than both l_1-norm minimization and RefCS by a factor of 9.35 on average.

5.2 Video Sequence Reconstruction

In this section, we explore the use of RefCS and RefCSLS in a case study of video sequence reconstruction. Consider a video sequence V as a collection of frames. Each frame $\mathbf{I}_t \in V$, $t = 1, 2, \ldots$, is a frame of V at time t. Each frame is compressively sampled using the sensing operation

$$\mathbf{y}_t = \mathbf{\Phi}\mathbf{\Psi}\mathbf{I}_t. \tag{35}$$

The reconstruction operation $\Re$ is employed to reconstruct the full frame $\hat{\mathbf{I}}_t$, obtained by

Fig. 7 Examples frames from (a) original sequences and sequences reconstructed from the 50% compressive measurements using (b) l_1-norm minimization method, (c) RefCS, and (d) RefCSLS.

$$\hat{\mathbf{x}}_t = \Re(\mathbf{y}_t, \mathbf{r}_t), \qquad (36)$$

$$\hat{\mathbf{I}}_t = \Psi^{-1}\hat{\mathbf{x}}_t. \qquad (37)$$

In this experiment, $\mathbf{r} = \hat{\mathbf{x}}_{t-1}$, with $\mathbf{r}_0$ being a vector of all zero with the same length as $\mathbf{x}$ is considered. The reconstruction operation is done using the conventional l_1-norm minimization and the proposed methods: RefCS and RefCSLS.

The example sequences used in this experiment are a set of 14 test video sequences. A few examples are displayed in Fig. 7(a). These sequences can be grouped into three categories based on the amount of activity they contain. These categories are low-, medium-, and high-activity sequences. Figure 7(b) shows the examples of the sequences reconstructed using the l_1-norm minimization, whereas Fig. 7(c) shows the sequences reconstructed using RefCS. The improvement of visual quality is obvious in the RefCS results compared to the results of conventional l_1-norm method. In particular, the RefCS results show the reduction of the noise-like reconstruction artifacts, which can be noticed easily in the l_1-norm minimization results. Figure 7(d) shows the examples reconstructed using RefCSLS. Even though RefCSLS does not promote the sparsity of the reconstruction

results and using a much less complex reconstruction method, it can be seen that the results of RefCSLS have the visual quality comparable to that of the regular RefCS results. These proposed methods clearly outperform the conventional l_1-norm minimization method in terms of visual quality.

Table 3 shows the objective comparison of the reconstruction quality of each reconstruction method using PSNR. Table 3 shows that the RefCS results have at least 40% higher in PSNR than the L_1-norm minimization. The use of the correlated reference contributes to the suppression of reconstruction artifacts Table 3 also shows the PSNR of the RefCSLS reconstructed video sequences. It shows that the quality of the RefCSLS reconstructed video sequences varies much greater than other methods. At the low sampling rate (such as 10%), the results of RefCSLS have poor PSNR compared to the conventional l_1-norm minimization. However, after the sampling rate increases beyond the crossover rate—empirically found to be 34% in this experiment— the quality of the RefCSLS reconstructed video outperforms that of the l_1-norm minimization reconstruction rapidly. At the sampling rate of 50%, the results from RefCSLS have on average 18% higher PSNR than the results of the l_1-norm minimization.

Table 3 Average PSNR in decibels of reconstructed sequences using the proposed reconstruction methods at the sampling rate of 10%, 30%, and 50%.

Methods	l_1-min			RefCS			RefCSLS		
	10%	30%	50%	10%	30%	50%	10%	30%	50%
Low-activity sequences									
Akiyo (01)	19.90	24.89	28.29	45.24	46.27	48.28	13.31	23.23	37.38
Claire (03)	18.07	24.25	28.37	30.97	34.30	38.60	12.45	22.82	35.06
Container (05)	18.47	22.59	25.94	37.87	40.39	43.57	9.76	20.12	34.35
Road (08)	21.87	27.26	31.32	32.87	34.76	37.78	8.59	18.77	31.87
Miss USA (10)	22.76	28.53	32.42	35.68	38.37	41.98	16.71	26.46	39.56
Medium-activity sequences									
Car (02)	16.94	22.17	26.13	26.85	28.74	31.93	12.10	21.12	28.82
Coastguard (04)	21.23	25.18	28.74	28.89	30.74	33.93	11.47	20.97	32.14
Office (07)	18.33	22.06	25.59	42.44	43.11	44.83	10.01	19.72	34.11
Mother (11)	20.32	26.09	29.73	41.14	41.91	44.30	11.75	22.20	35.86
News (12)	17.27	21.47	24.49	30.39	33.13	36.58	14.37	24.03	35.09
Salesman (13)	20.29	24.24	27.63	35.43	37.29	39.99	15.50	24.57	32.34
High-activity sequences									
Foreman (06)	17.17	21.89	26.04	23.93	24.04	31.23	8.88	18.22	28.14
Skates (09)	15.71	20.51	24.14	15.47	19.15	23.28	9.55	15.90	20.25
Silence (14)	19.04	23.52	27.28	39.97	41.41	44.11	10.66	20.69	33.29

It can be noticed in Table 3 that the performance of RefCS is inversely proportional to the amount of activity in the sequences. The reason for this is the larger reference distance δ in the high-activity sequences that consist of lots of movements. The amount of activity does not affect the performance of the l_1-norm minimization, though, as each frame is reconstructed independently from each other. As the reconstruction error of RefCS is bounded by Proposition 2, RefCS is guaranteed to outperform the l_1-norm minimization when the reference distance δ is closer to the signal than the l_1-norm solution by a factor of two. A sequence containing lots of movement could lead to a reference that is too distant to the signal, thus, reducing the performance of RefCS. Also since the reconstructed preceding frame is used as the reference, the errors are propagated to successive frame reconstructions leading to more artifacts in later frames. One can avoid this by introducing an l_1-norm minimization-based reconstructed frame for every group of frames in a similar manner to introducing an intraframe in conventional video coding algorithms.

Finally, Table 4 shows the average reconstruction time per frame for each sequence using each method. As discussed in Sec. 4, because RefCSLS does not use an iterative algorithm, it results in a shorter reconstruction time by the factor of at least 1200 compared to that of RefCS and l_1-min.

Table 4 Average reconstruction time per frame (s) of each reconstruction method.

Methods	Reconstruction time per frame (s)		
	l_1-min	RefCS	RefCSLS
Low-activity sequences			
Akiyo	2.3	2.24	1.7×10^{-3}
Claire	2.17	2.18	1.8×10^{-3}
Container	2.11	2.29	1.9×10^{-3}
Road	2.18	2.19	1.7×10^{-3}
Miss USA	2.16	2.18	1.8×10^{-3}
Medium-activity sequences			
Car	2.22	2.21	1.8×10^{-3}
Coastguard	2.17	2.22	1.8×10^{-3}
Office	2.17	2.30	2.0×10^{-3}
Mother	2.23	2.20	1.8×10^{-3}
News	2.13	2.17	1.8×10^{-3}
Salesman	2.15	2.14	1.8×10^{-3}
High-activity sequences			
Foreman	2.16	2.26	1.7×10^{-3}
Skates	2.15	2.15	1.8×10^{-3}
Silence	2.17	2.18	1.7×10^{-3}

5.3 Functional Magnetic Resonance Imaging Data Reconstruction

In this section, we explore another case study of RefCS and RefCSLS in fMRI data reconstruction. Unlike conventional MRI, fMRI requires a series of several three-dimensional tomographic volumes in order to extract the region of brain activity of a subject. The use of compressed sensing in fMRI offers the benefit of a better trade-off between the image quality and the acquisition time, i.e., higher resolution data can be obtained as fast as the current high-speed low-resolution scan.

The spatio-temporal nature of fMRI data fits perfectly with the proposed paradigm. The aim of this section is to reconstruct a series $\mathcal{S}$ consisting of full three-dimensional volumes. Each volume $\mathbf{V}_t \in \mathcal{S}$, $t = 1,2,\ldots$, is to be reconstructed from its compressive measurements $\mathbf{y}_t = \mathfrak{S}(\mathbf{x}_t)$, where $\mathbf{x}_t$ is the complete K-space of $\mathbf{V}_t$. Suppose that the sensing operation $\mathfrak{S}(\mathbf{x}_t) = \mathbf{\Phi}\mathbf{x}_t$ is built into the scanning procedure, the reconstructed volume $\hat{\mathbf{V}}_t$ can be obtained from

$$\hat{\mathbf{V}}_t = \mathbf{\Psi}^{-1}\hat{\mathbf{x}}_t, \tag{38}$$

where

$$\hat{\mathbf{x}}_t = \Re(\mathbf{y}_t, \mathbf{r}), \tag{39}$$

$\mathbf{r} = \hat{\mathbf{x}}_{t-1}$, and $\mathbf{\Psi}^{-1}$ is the inverse Fourier transform.

To demonstrate this, a set of fMRI data is reconstructed from the simulated compressive measurements of their K-space. The fMRI data used in this experiment are from the following datasets:

1. attention to visual motion dataset[38] (DS1),
2. auditory fMRI dataset[38] (DS2),
3. mixed-gambles task fMRI dataset (obtained from the OpenfMRI database with accession number ds000005[39]) (DS3), and
4. visual object recognition dataset (obtained from the OpenfMRI database with accession number ds000105[40]) (DS4).

Each data point is reconstructed from the compressive measurements of 10%, 30%, and 50%. Figure 8(a) shows the example slices from each dataset.

First, Figs. 8(b)–8(d) present the examples slices of the reconstructed data employing different reconstruction methods for the purpose of subjective evaluation of the visual quality. It is clear that, at the sampling rate of 50%, both RefCS [Fig. 8(c)] and RefCSLS [Fig. 8(d)] outperform the conventional l_1-norm minimization method. Even though the l_1-norm minimization fails to reconstruct the small details, particularly in the DS2 and DS4, these details, however, are clearly preserved using the proposed methods.

To evaluate the visual quality objectively, Table 5 shows the average PSNR of the reconstructed fMRI data. Table 5 confirms the observation made in the subjective evaluation that the RefCS outperforms the conventional l_1-norm minimization, resulting in 90% higher PSNR on average. More interesting results are the reconstructed data using RefCSLS. Table 5 shows that the performance of RefCSLS in reconstructing fMRI data is comparable to the regular RefCS, despite having much less computational complexity. In contrast to the results of video reconstruction, shown in Sec. 5.2, here the performance of RefCSLS does not drop below that
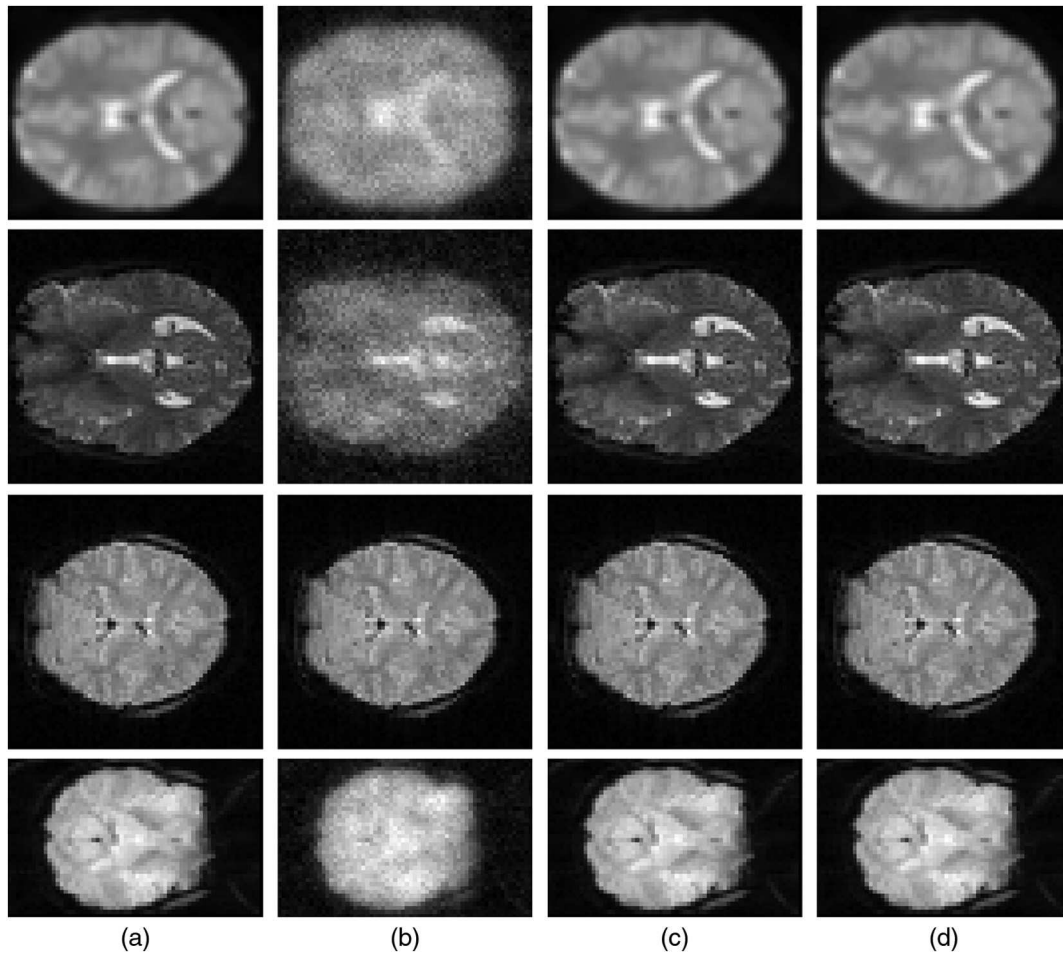
Fig. 8 Examples of the reconstructed data using different reconstruction methods from the compressive measurements with the sampling rate of 50%: (a) original lossless data, (b) l_1-norm minimization, (c) RefCS, and (d) RefCSLS.

of the l_1-norm minimization at low sampling rate. The reason for this dramatic improvement lies in the characteristic of the fMRI data. Unlike in natural video sequences, the difference between two consecutive volumes is largely due to the changes of the intensity of each voxel rather than movements. This

results in a much smaller reference distance δ in fMRI data, thus, improving the performance of the proposed methods dramatically. On average, the data reconstructed using RefCSLS results in 89% higher PSNR, and the reconstruction time is shortened by the factor of 5.4×10^4, as shown in Table 6.

Table 5 Average PSNR of data reconstructed using different reconstruction methods.

Method	Sampling rate (%)	DS1	DS2	DS3	DS4
l_1-min	10	24.97	16.22	26.35	21.79
	30	25.56	24.94	34.86	26.03
	50	32.87	25.24	36.17	30.21
RefCS	10	56.35	41.19	50.86	44.69
	30	60.14	42.85	52.25	46.11
	50	65.23	44.78	54.63	48.01
RefCSLS	10	56.05	41.27	51.03	44.92
	30	57.60	42.86	52.60	46.48
	50	59.59	44.84	53.75	48.45

Table 6 Average reconstruction time per volume (s) using different reconstruction methods.

Method	Sampling rate (%)	DS1	DS2	DS3	DS4
l_1-min	10	218.91	374.28	206.66	194.34
	30	391.42	602.31	380.46	310.78
	50	641.68	874.00	662.47	513.71
RefCS	10	214.32	373.63	208.13	194.93
	30	383.95	579.32	385.86	310.87
	50	636.43	872.67	660.37	496.87
RefCSLS	10	0.41	0.53	0.35	0.27
	30	0.92	1.22	0.77	0.72
	50	1.21	1.71	1.15	1.08

6 Conclusions

In this paper, we have presented a framework for using a reference signal for compressed sensing reconstruction. The proposed algorithm, RefCS, improves the reconstruction quality of the compressed sensed signals by exploiting the spatial- or temporal-redundancy of the correlated reference. We have shown that RefCS outperforms the conventional l_1-norm minimization method in terms of PSNR in three different scenarios, i.e., the multiscale image reconstruction, video sequence reconstruction, and fMRI data reconstruction. By exploiting the correlated reference, RefCS can improve the reconstruction quality by up to 90% in terms of PSNR in the experiments. For video sequences, the proposed method is more efficient when the amount of motion is low, as there is no motion compensation is utilized in the proposed paradigm.

We also demonstrated that by using a correlated reference it was possible to reconstruct the signals using the least squares method. The results using RefCSLS are comparable to those from the regular RefCS in terms of PSNR, while being able to obtain the results much faster than the conventional iterative reconstruction algorithms, for example, improving the reconstruction time by a factor ranging from 9 to 5.4×10^4 in our experiments. With the proposed methods, this paper has successfully addressed two challenges of applying compressed sensing in a practical application, namely, its poor reconstruction quality and its high computational complexity.

References

1. E. J. Candès, J. Romberg, and T. Tao, "Robust uncertainty principles: exact signal reconstruction from highly incomplete frequency information," *IEEE Trans. Inf. Theory* **52**, 489–509 (2006).
2. D. L. Donoho, "Compressed sensing," *IEEE Trans. Inf. Theory* **52**, 1289–1306 (2006).
3. E. J. Candès and M. B. Wakin, "An introduction to compressive sampling," *IEEE Signal Process. Mag.* **25**, 21–30 (2008).
4. A. Cohen, W. Dahmen, and R. DeVore, "Compressed sensing and best k-term approximation," *J. Am. Math. Soc.* **22**(1), 211–231 (2009).
5. E. J. Candès and J. Romberg, "Sparsity and incoherence in compressive sampling," *Inverse Prob.* **23**, 969–985 (2007).
6. E. Candès, "The restricted isometry property and its implications for compressed sensing," *C. R. Math.* **346**, 589–592 (2008).
7. K. Kim and G. Shevlyakov, "Why Gaussianity?" *IEEE Signal Process. Mag.* **25**, 102–113 (2008).
8. M. Lustig et al., "Compressed sensing MRI," *IEEE Signal Process. Mag.* **25**, 72–82 (2008).
9. J. P. Haldar, D. Hernando, and Z. P. Liang, "Compressed-sensing MRI with random encoding," *IEEE Trans. Med. Imaging* **30**, 893–903 (2011).
10. H. Hu and Z. Yang, "Spatial correlation-based distributed compressed sensing in wireless sensor networks," in *Proc. 2010 6th Int. Conf. Wirel. Commun. Networking Mob. Comput. (WiCOM)*, IEEE, 1–4 (2010).
11. V. Thirumalai and P. Frossard, "Joint reconstruction of multi-view compressed images," *IEEE Trans. Image Process.* **22**(5), 1969–1981 (2012).
12. G. Warnell, D. Reddy, and R. Chellappa, "Adaptive rate compressive sensing for background subtraction," in *Proc. 2012 IEEE Int. Conf. Acoust. Speech and Signal Process. (ICASSP)*, pp. 1477–1480 (2012).
13. C. Miosso, R. von Borries, and J. Pierluissi, "Compressive sensing with prior information requirements and probabilities of reconstruction in l1-minimization," *IEEE Trans. Signal Process.* **61**(9), 2150–2164 (2013).
14. J. F. C. Mota, N. Deligiannis, and M. R. D. Rodrigues, "Compressed sensing with side information: geometrical interpretation and performance bounds," in *IEEE Global Conf. Signal Inf. Process. (GlobalSIP)*, pp. 512–516 (2014).
15. J. Scarlett, J. S. Evans, and S. Dey, "Compressed sensing with prior information: information-Theoretic limits and practical decoders," *IEEE Trans. Signal Process.* **61**, 427–439 (2013).
16. R. Baraniuk et al., "Model-based compressive sensing," *IEEE Trans. Inf. Theory* **56**(4), 1982–2001 (2010).
17. N. Vaswani, "Kalman filtered compressed sensing," in *Proc. 15th IEEE Int. Conf. Image Process. (ICIP)*, pp. 893–896 (2008).
18. D. Jones, R. Schlick, and R. Marcia, "Compressive video recovery with upper and lower bound constraints," in *Proc. 2012 IEEE Int. Conf. Acoust. Speech Signal Process. (ICASSP)*, pp. 3325–3328 (2012).
19. X. Zhu, L. Zhang, and Y. Liu, "Scalable distributed video coding using compressed sensing in wavelet domain," in *Proc. 18th IEEE Int. Conf. Image Process. (ICIP)*, pp. 2677–2680 (2011).
20. L. Kang and C. Lu, "Distributed compressive video sensing," in *Proc. 2009 IEEE Int. Conf. Acoust. Speech and Signal Process. (ICASSP)*, pp. 1169–1172 (2009).
21. V. Stankovic, L. Stankovic, and S. Cheng, "Compressive video sampling," in *Proc. Eur. Signal Process. Conf. (EUSIPCO)*, pp. 2–6 (2008).
22. C. Ma et al., "Distributed compressive video sensing based on smoothed l0 norm with partially known support," in *Proc. 2011 IEEE Int. Conf. Multimedia and Expo*, pp. 1–6 (2011).
23. L. Liu et al., "An improved distributed compressive video sensing based on adaptive sparse basis," in *Proc. 2011 First Int. Conf. Robot, Vision and Signal Process.*, pp. 137–140 (2011).
24. H. Yin et al., "Efficient multiple frame images recovery based on distributed compressed sensing," in *Proc. 2014 World Autom. Congress (WAC)*, pp. 834–840 (2014).
25. S. Kurihara and H. Kikuchi, "An improvement of key frame processing by an integration of compressive sensing and intra prediction of H.264/AVC," in *Proc. 2014 IEEE Region 10 Symp.*, pp. 584–587 (2014).
26. X. Yuan et al., "Adaptive temporal compressive sensing for video," in *Proc. 2013 IEEE Int. Conf. Image Process.*, pp. 14–18 (2013).
27. J. Yang et al., "Video compressive sensing using Gaussian mixture models," *IEEE Trans. Image Process.* **23**, 4863–4878 (2014).
28. L. Weizman, Y. C. Eldar, and D. Ben Bashat, "Compressed sensing for longitudinal MRI: an adaptive-weighted approach," *Med. Phys.* **42**(9), 5195–5208 (2015).
29. L. Weizman et al., "Exploiting similarity in adjacent slices for compressed sensing MRI," in *Proc. 2014 36th Ann. Int. Conf. IEEE Eng. Med. Biol. Soc. (EMBC)*, pp. 1549–1552 (2014).
30. J. Park and M. Wakin, "A multiscale framework for compressive sensing of video," in *Proc. 2009 Picture Coding Symp.*, pp. 1–4 (2009).
31. Z. Gao, C. Xiong, and C. Zhou, "Random permutations based block compressive sensing for image compression applications," in *18th IEEE Int. Conf. Image Process. (ICIP)*, pp. 293–296 (2011).
32. N. Onhon and M. Cetin, "A sparsity-driven approach for joint SAR imaging and phase error correction," *IEEE Trans. Image Process.* **21**(4), 2075–2088 (2012).
33. W. Hotrakool and C. Abhayaratne, "Fast compressed sensing reconstruction using the least squares and signal correlation," in *IET Intell. Signal Process. Conf. (ISP 2013)*, pp. 1–6 (2013).
34. W. Hotrakool and C. Abhayaratne, "Running Gaussian reference-based reconstruction for video compressed sensing," in *IEEE Int. Conf. Acoust., Speech Signal Process. (ICASSP)*, pp. 2001–2005 (2014).
35. W. Hotrakool, "Compressed sensing for functional magnetic resonance imaging data," PhD thesis, University of Sheffield, United Kingdom (2018) http://etheses.whiterose.ac.uk/id/eprint/15704.
36. D. A. Lorenz, M. E. Pfetsch, and A. M. Tillmann, "An infeasible-point subgradient method using adaptive approximate projections," *Comput. Optim. Appl.* **57**(2), 271–306 (2013).
37. D. A. Lorenz, M. E. Pfetsch, and A. M. Tillmann, "Solving basis pursuit: heuristic optimality check and solver comparison," *ACM Trans. Math. Software* **41**, 1–29 (2015).
38. C. Buchel and K. J. Friston, "Modulation of connectivity in visual pathways by attention: cortical interactions evaluated with structural equation modelling and fMRI," *Cereb. Cortex* **7**(8), 768–778 (1997).
39. S. M. Tom et al., "The neural basis of loss aversion in decision-making under risk," *Science* **315**(5811), 515–518 (2007).
40. A. J. O'toole et al., "Partially distributed representations of objects and faces in ventral temporal cortex," *J. Cognit. Neurosci.* **17**(4), 580–590 (2005).

Wattanit Hotrakool received his MS degree in computer vision engineering and PhD in electronics and electrical engineering from the University of Sheffield, United Kingdom, in 2011 and 2016, respectively. He was a postdoctoral research associate at the University of Sheffield in 2017. His main research interests include the analysis of medical image data, sparse signal reconstruction, object recognition, and machine learning.

Charith Abhayaratne received his BE degree in electrical and electronic engineering (EEE) from the University of Adelaide, Australia, in 1998, and his PhD in EEE from the University of Bath, UK, in 2002. He received the European Research Consortium for Informatics and Mathematics Postdoctoral Fellowship in 2002. He is a lecturer in the Department of EEE at the University of Sheffield, UK. He has published more than 70 peer-reviewed papers in signal processing, image and video compression, multimedia security, and computer vision.